We are IntechOpen, the world's leading publisher of Open Access books
Built by scientists, for scientists

4,800
Open access books available

122,000
International authors and editors

135M
Downloads

Our authors are among the

154
Countries delivered to

TOP 1%
most cited scientists

12.2%
Contributors from top 500 universities

CLARIVATE ANALYTICS
BOOK CITATION INDEX
INDEXED

WEB OF SCIENCE™

Selection of our books indexed in the Book Citation Index in Web of Science™ Core Collection (BKCI)

Interested in publishing with us?
Contact book.department@intechopen.com

Numbers displayed above are based on latest data collected.
For more information visit www.intechopen.com

Chapter 6

Perspective of Additive Manufacturing Selective Laser Melting in Co-Cr-Mo Alloy in the Consolidation of Dental Prosthesis

Marcello Vertamatti Mergulhão,
Carlos Eduardo Podestá and
Maurício David Martins das Neves

Additional information is available at the end of the chapter

http://dx.doi.org/10.5772/intechopen.69720

Abstract

This chapter seeks to compare the properties of samples manufactured by additive manufacturing (AM) by the selective laser melting (SLM) technology and compare with the precision casting (PC) processes using the Co-Cr-Mo (ASTM F75) alloy to manufacture of dental prosthesis. This AM process can be manufactured three-dimensional models by means of a laser beam that completely melts particles of powder deposited layer by layer. However, it is still relevant to know the properties of: performance, dimensional, mechanical and microstructural of this laser melting process and compare with a convencional process. The results of mechanical evaluation showed that the SLM technique provides superior mechanical properties compared to those obtained by the PC technique. It is possible to verify that the consolidation by SLM technique results in lower presence of porosity than PC technique. In addition, PC samples presented a gross dendritic microstructure of casting process. Microstructural analysis of SLM samples results in a characteristic morphology of layer manufacturing with ultrafine grains and a high chemical homogeneity. In this way, the development of the present study evidenced to improve the manufacture of customized components (copings) using the SLM technology.

Keywords: Co-Cr-Mo alloy, biomaterial, additive manufacturing, selective laser melting, precision casting

INTECH
open science | open minds

© 2018 The Author(s). Licensee InTech. This chapter is distributed under the terms of the Creative Commons Attribution License (http://creativecommons.org/licenses/by/3.0), which permits unrestricted use, distribution, and reproduction in any medium, provided the original work is properly cited. CC BY

1. Introduction

Metal powders of cobalt-chromium (Co-Cr) alloy are widely used in various sectors of the automotive, aeronautics, and aerospace industry, because of its high wear resistance and adequate corrosion resistance also being used in surface coating to increase performance components [1, 2]. In addition, the biocompatibility properties are suitable and are being used in the manufacture of medical and dental prosthetics [3–7]. The use of Co-Cr alloys is widely discussed to manufacture medical and dental implants or prostheses [7–9] presenting positive aspects in relation to biocompatibility analysis. The necessity for characterization and biological evaluations, physical-chemical, and mechanical are basic requirements for the development of new biomaterials applied in medical devices. In general, biomaterials need to present a final clinical characteristic (bio-functionality) and biocompatibility [10, 11].

Since 1930, Cobalt-Chromium-Molybdenum (Co-Cr-Mo) alloys processed by casting were used as dental alloys and later adapted for use in orthopedic implants [12, 13]. According to Jabbari et al., Co-Cr alloys are used almost exclusively in the manufacture of metal structures prostheses and recently is replacing Ni-Cr alloy or alternatively for the production of restorations in porcelain fused to metal (PFM), because Co-Cr alloy is Ni-free and does not have allergic responses or toxic effects related to Nickel [14].

The coefficient of thermal expansion (CTE) is a thermal property of the alloy, is of great interest in cases of applications in dental components, that requires ceramic coating, such as the dental crown. In this case, it is shown by Refs. [6, 15, 16] that Co-Cr alloys should have a CTE value in the range of 14.0–14.6 × 10^{-6} °C^{-1} at temperatures from 500 to 600°C to the correct ceramic firing process, as coating of the metal component. The CTE of ceramic materials for coating applications in metallic materials should be close, providing a good adjustment due to contraction and expansion during heating, thus avoiding the possibility of voids or cracks occurring during the firing process [15, 17].

Currently, the lost wax casting method is the most widely used, but has faced competition from other manufacturing processes [17]. Several authors [18–20] describe the development of AM technologies providing the creation of final customized implants. Techniques such as stereolithography were implemented to manufacture resin models for posterior manufacture of dental prostheses (crowns and bridges) by conventional process of lost wax castings. Mechanical, chemical, and microstructural properties are evaluated in comparison to new AM technologies, for example, the selective laser melting (SLM) in relation to conventional techniques as lost wax casting [21–23]. In this way, the preparation of medical and dental components provides customized final components with high mechanical properties, compared to conventional techniques (see **Figure 1**) [24].

Notably in health area, this technology is competitive over other traditional manufacturing processes by advances occurred in the area of processes using powder metallurgy techniques [25, 26]. Selective laser melting technology is one of the innovative technologies in additive manufacturing development in the middle of the 1980s after the creation of selective laser sintering (SLS) process. SLM is a process based on the 3D construction in which it is possible by laser beam to completely melt the metallic powder particles on a previous layer [27–31].

http://dx.doi.org/10.5772/intechopen.69720

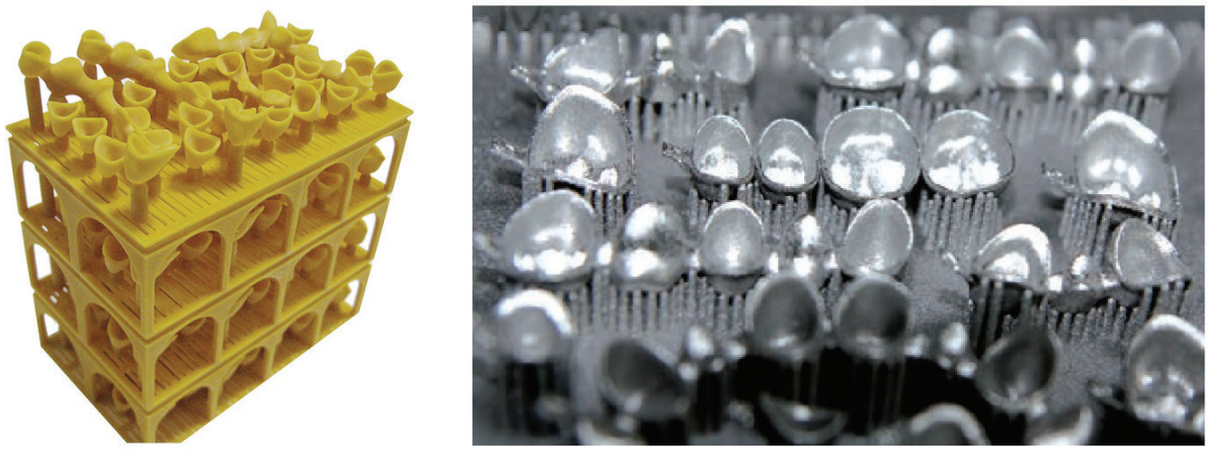

Figure 1. Models of dental components manufactured by AM techniques in (a) resin model by stereolithography for posterior precision casting process and (b) copings manufactured by SLM technique [17].

In SLM technique, the raw material is in metallic powder form and the thermal energy required for the complete melting of the powder layer comes from a laser beam, usually is used a source of Ytterbium (Yb) fiber [29]. The maximum laser power on SLM machines is approximately 400 W and the laser focus may have a diameter of approximately 100 μm [30]. In turn, the laser beam is commanded by an interface that transmits it to the optical assembly, which selectively directs (X–Y plane) the laser beam, causing the powders to melt [28–33]. The metal powder is stored in a container, which may or may not be the distributor of powder (deposited by gravity), which in turn uniformizes the powder layer (between 50 and 100 μm) on an object consolidation platform. At each consolidated layer, the platform moves on the Z–axis, according to the next layer until the component is completely consolidated. The process of component consolidation occurs in a consolidation chamber (internal environment of the SLM equipment) that is under inert atmosphere protection (argon gas) [28–33]. The basic scheme of the components present in the consolidation process by SLM can be observed in **Figure 2**, and other machine parameters and working conditions are presented in **Table 1**.

Details of the main parameters of the SLM technique are shown schematically in **Figure 3**.

The SLM technique has several process parameters and can be grouped in five families, being these related to laser, scanning, material (powder), temperature, and consolidation chamber [28, 29, 31].

- Laser: power "P", beam diameter, pulse duration, pulse frequency;
- Scanning: speed "v", track distance, strategy;
- Powder (material): material properties, particle size, distribution, bed density of powder, layer thickness;
- Temperature: consolidation layer, powder feeder, uniformity;
- Compounding chamber: composition of protective atmosphere.

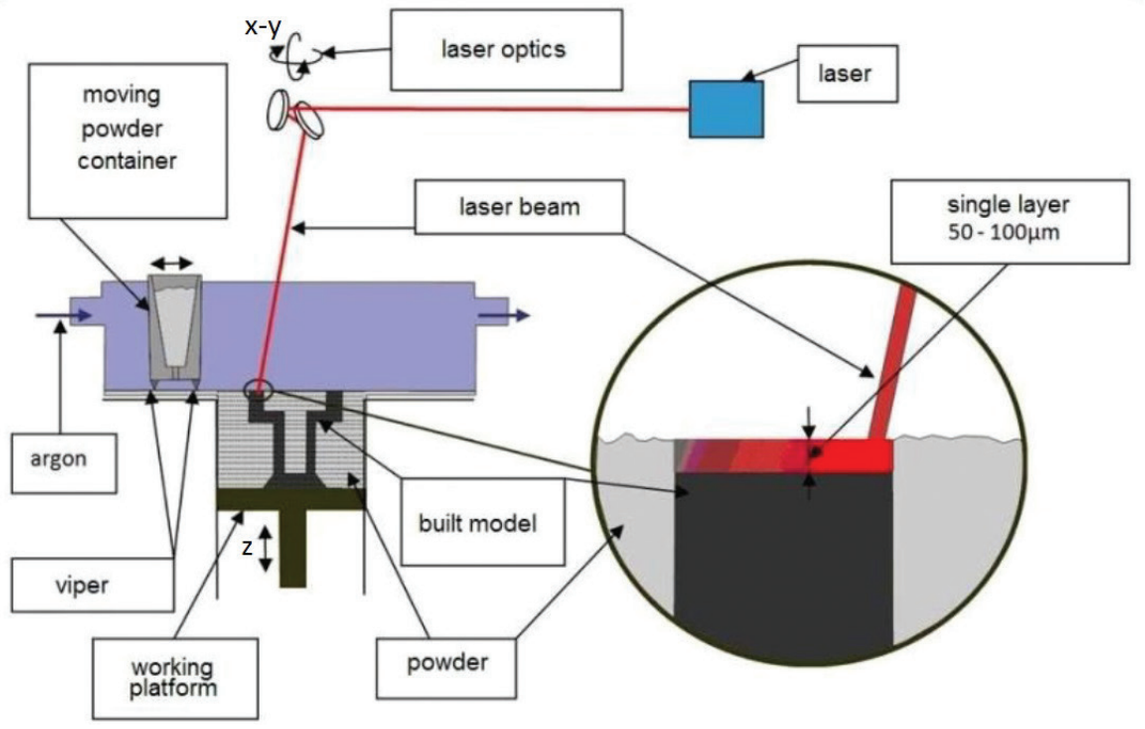

Figure 2. Basic schematic of components present in a SLM machine [33].

The most common parameters to be adjusted in the SLM process to optimize the manufacture of components are: laser power (P), scan speed (v), track (hatch) distance, and layer thickness. According to Refs. [27, 34, 35], the volumetric energy density of the laser (ψ, given in J.mm^{-3}) relates the main parameters of consolidation, in relation to the laser as shown in Eq. (1), being: laser power (P), track distance (t), scan speed (v), and layer thickness (L).

$$\psi = \frac{P}{t \cdot v \cdot L} \tag{1}$$

System parameters	
Laser power	400 W Yb-Fiber-laser
Build speed	20 ccm/h
Pract. layer thickness	20–75 µm min
Scan line/wall thickness	150 µm
Operational beam focus	80–120 µm
Scan speed	15 m/s
Inert gas consumption in operation	Ar/N_2, 2.5–3.0 l/min
Inert gas consumption venting	Ar/N_2, 1700 l @ 100 l/min
Compressed air requirement	18 l/min @ 1.5 bar

Table 1. Typical technical parameters of the SLM®280^{HL} machine.

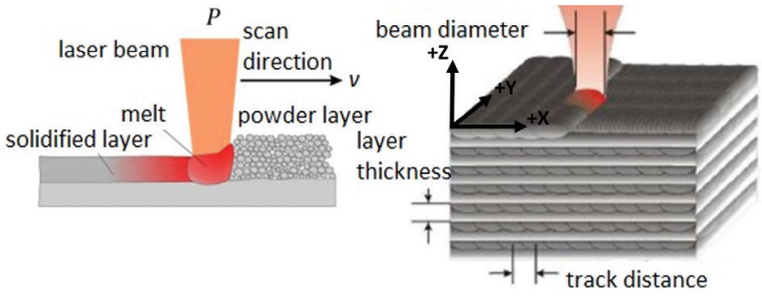

Figure 3. Schematic of parameters involved in SLM consolidation [31].

Several authors in Refs. [27, 34, 35] report that these parameters affect the volumetric energy density, determinant in the powder melting and that in turn influences the mechanical properties and roughness of the surface of the consolidated parts. The combination of these variables can generate excess (or insufficient) energy during the consolidation process, which can lead to the balling phenomenon at consolidated specimen, which corresponds to the dissimilar or noncontinuous scan tracks [30, 36, 37]. Additionally, the balling phenomenon can generate uniform deposition of next powder layer, can cause uncontrollable porosity and delamination by the absence of inter-fusion between layers [37, 38].

As observed, the parameters of the SLM process involve a certain complexity, in order to obtain the fabrication of components of complete density. In order to optimize the mechanical and physical-chemical properties of the final components manufactured the consolidation strategies are the subject of discussion and study [39]. The consolidation strategies refer to the consolidation parameters already presented, as well as to the direction and orientation of laser beam scanning, angle of rotation between the layers, and the number passes of laser beam (per layer), as seen in **Figure 4a–h** [40–42]. Also, the physical properties of the components may be associated with the manufacturing anisotropy of the samples, see **Figure 4i** [43–45].

An interesting point to consider for AM processes is the feedstock (or raw material–metal powder). These new technologies demanded a characteristic powder size distribution, format and physical properties (flowability and packing) [36]. In this case, to produce spherical metal powder the most common process is gas atomization [29, 30]. However, it is remarkable that the use of gas-atomized powders in the SLM process by the better physical properties is compared to water-atomized powders. The characteristic format of powders (gas and water atomized) is possible to observe in **Figure 5**.

In addition, the capability to reusability of feedstock material in AM processes is a significant issue to promote economic and environmental manufacture processes [28, 46]. However, the effects and influence of the powder reuse on manufactured parts are the subject of much discussion [47–50]. The conclusions of Tang et al. [48] study, about reuse of Ti-6Al-4V powders of electron beam melting (EBM) process, appoint the increased oxygen content and particles became less spherical. Although the reuse powder improved the flowability (by little presence of satellite particles), increased the yield strength and the ultimate tensile on the AM process of Ti-6Al-4V [48].

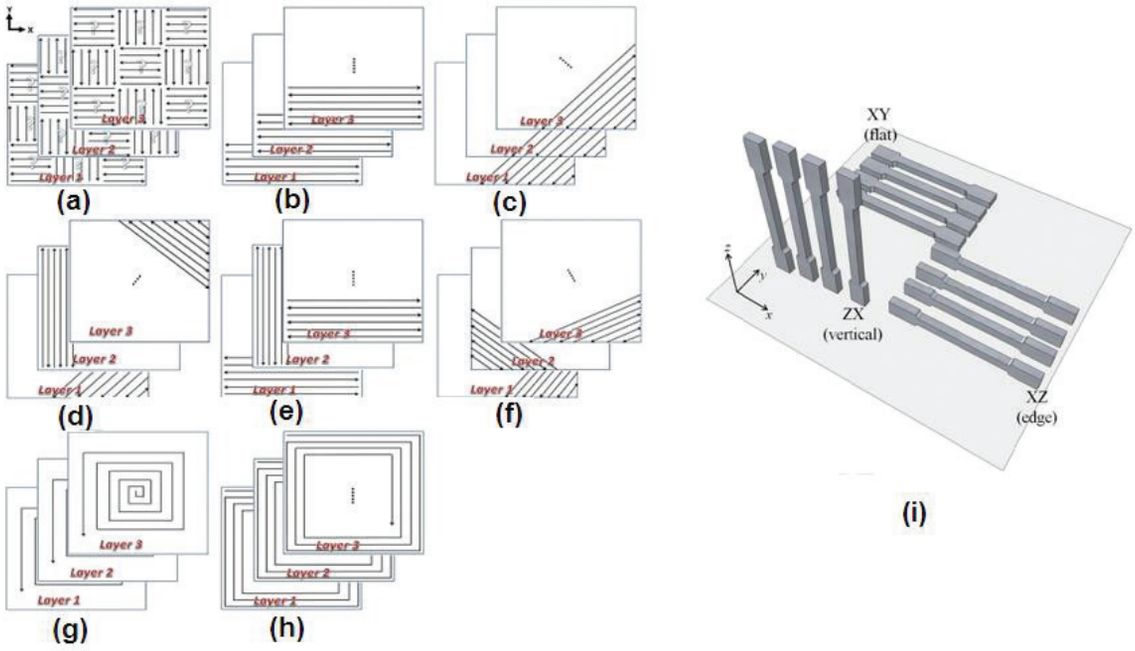

Figure 4. Representation of laser scanning strategies for sample consolidation via SLM, scanning in: (a) island, (b) line, (c) line at 45°, (d) line and rotation line at 45°, (e) line and rotation line at 90°, (f) line rotate at 67°, (g) internal spiral, (h) external spiral [42], and (i) building orientation of specimens [45].

Considering this important field in expansion, this chapter is part of this scenario with a focus on the dental sector, more specifically on the evaluation of mechanical properties and microstructural analysis of Co-Cr-Mo alloy to manufacture dental prostheses (copings). The aim of this chapter is to evaluate the mechanical properties and microstructures of standardized specimens made by powder metallurgy techniques using SLM from powdered gas powder of the Co-Cr-Mo alloy. The results obtained by SLM will be compared with the results of samples manufactured by precision casting.

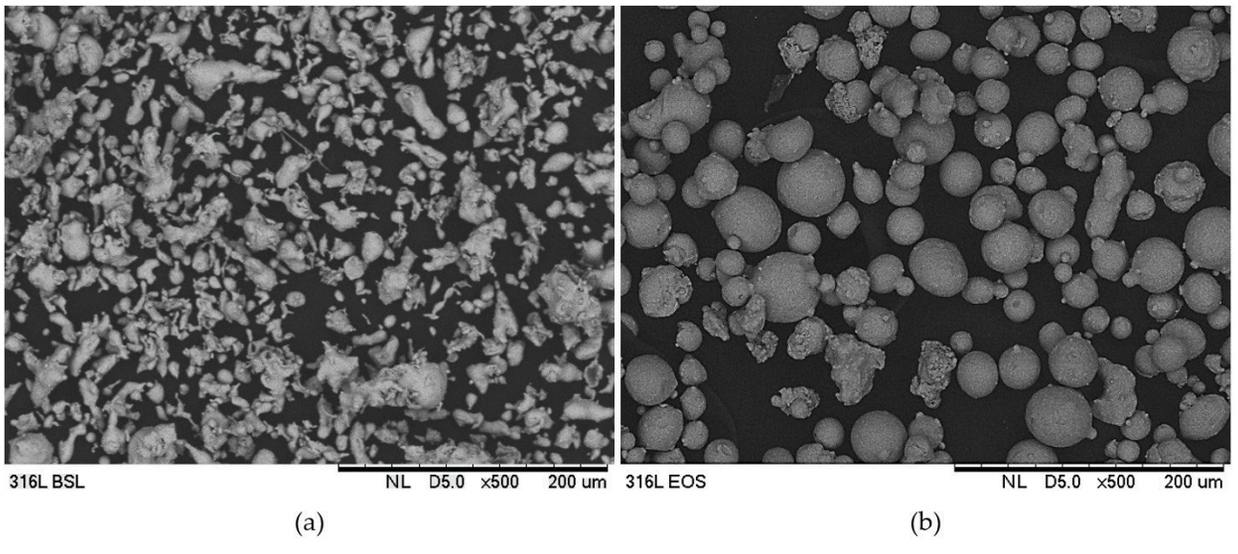

Figure 5. Characteristic format of powders (316L alloy) produced by water atomization (a) and gas atomization (b). Magnitude ×500.

http://dx.doi.org/10.5772/intechopen.69720

2. Experimental procedure

2.1. Powder characterization

Co-Cr-Mo alloy gas atomized (H.C Starck®, Lübeck, Germany) was provided by the HighBond® (Indaiatuba, Brazil) in the particle size (granulometric range) of 15–45 μm. The confirmation of the chemical composition was performed by energy dispersive X-ray (Shimadzu EDX-720 equipment and by LECO). This study was based on alloy/powder with certification of ANVISA (Brazilian agency) for use in health care segment.

Several physical properties of gas-atomized powder were obtained such as flow time (ASTM B212 [51]), apparent density (ASTM B213 [52]), and tap density (ASTM B527 [53]). The particle size distribution was performed using a particle analyzer by laser scattering (Cilas–Model 1064). The particle format and microstructural characterization of powders were performed via optical and scanning electron microscopy (OM–Olympus BX51M and SEM-EDS Philips XL30).

To evaluate the internal porosity of powders sample were measured by the pycnometer density in comparison to theoretical density. The density by Helium pycnometry considered only the internal porosity (excluding the open porosity) and was performed using the Micromeritics equipment (Model Accu PYC 1330 Pycnometer).

Differential scanning calorimetry (DSC) analysis was performed using a sample of gas-atomized Co-Cr-Mo powder. Three runs of heating curves at rates of 10, 20, and 30°C/min were performed and under static atmosphere constituted in argon (99.999%) for minimizing the oxidation of the samples. In all experiments, both the crucible (sample holder and the reference–empty during all tests) were composed of alumina (Al_2O_3) with a volume of approximately 100 μL. The equipment used was Setsys 16/18, from Setaram with a thermocouple rod of Pt/Pt Rh 10%.

2.2. Manufacturing specimens using precision casting and selective laser melting

Precision casting and selective laser melting techniques performed the manufacture of gas-atomized Co-Cr-Mo powders. The tensile and three-point bending specimens were manufactured in standard dimensions according to ISO 22674-06 [54] and ASTM B528-12 [55]. **Figure 6** shows specimens manufactured.

The precision casting (PC) samples were performed according to ASTM F75-12 [13] by HighBond® (Indaiatuba, Brazil). The PC fabrication process method satisfied the following steps: machining of wax disks in the standard dimensions of tensile and flexural test specimens, assembly and shell building, dewaxing and pouring the Co-Cr-Mo alloy was by an induction furnace at a temperature of 1489°C.

The consolidation of SLM samples was carried out by SLM Solutions™ using a selective laser melting machine SLM®280HL with a single Ytterbium laser beam (maximum power 400 W). The building consolidation of specimens was parallel to laser beam and performed using parameters such as: layer thickness of 30 μm and diameter of laser beam of 76 μm.

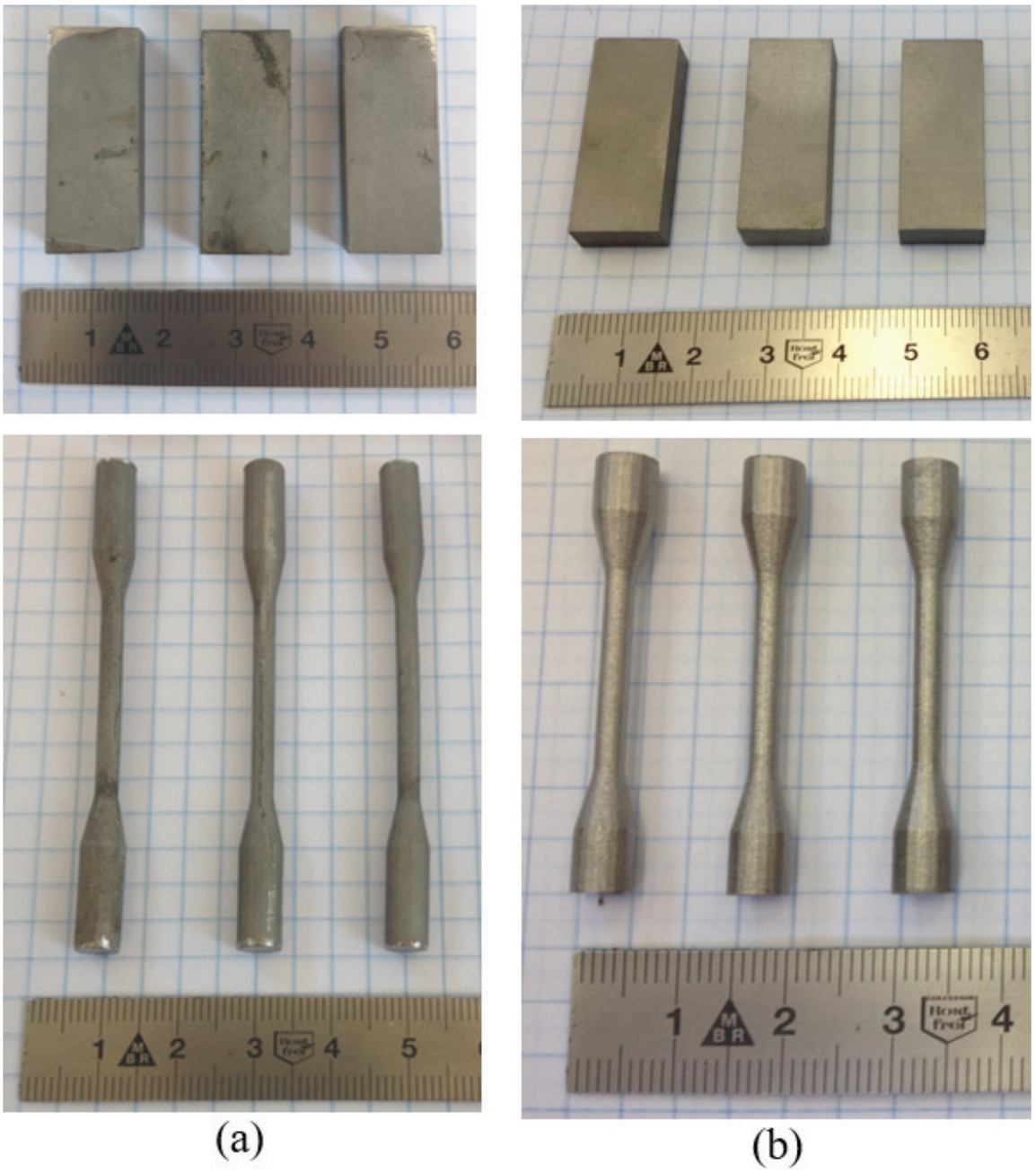

Figure 6. Specimens manufactured of Co-Cr-Mo alloy: (a) specimens made by FP technique and (b) specimens made by SLM technique.

2.3. Characterization of samples manufactured

To evaluate the susceptibility to cell growth in the Co-Cr-Mo alloy after the consolidation processes (PC and SLM) was performed by the cytotoxicity analysis, according to ISO 10993-5 [56]. The determination of the cytotoxicity was obtained by the quantitative evaluation method, which is carried out by the measurement of cell death, cell proliferation or formation of cellular colonies.

To evaluate the internal porosity of cast, and SLM samples were measured by the pycnometry density in comparison to the theoretical density. The density by Helium pycnometry, considered only the internal porosity (excluding the open porosity) was measured using the Micromeritics equipment–Model Accu PYC 1330 Pycnometer.

The thermomechanical analysis (TMA) was performed on samples consolidated by SLM and PC of the Co-Cr-Mo alloy. The purpose of the technique was to obtain the coefficient of thermal expansion (CTE). In addition, the SLM samples were analyzed in the parallel and transversal building direction (SLM 1—parallel direction and SLM 2—transversal direction). The routine of the TMA remained the heating rate was from 10°C/min until the temperature of 1300°C. The equipment used was a Setaram–Setsys 16/18, using a thermocouple rod of Pt/Pt Rh 10% under a static atmosphere (argon—99.999%) to exclude the sample oxidation.

2.4. Mechanical characterization

Mechanical characterization of consolidated samples by PC and SLM techniques was held in five samples of each test (tensile and three-point bending), respectively, according to ISO 22674-06 [54] and ASTM B528 [55]. The three-point bending test determined the transversal rupture strength (TRS) of specimens. The TRS relates to the applied load (P) and the distance between the supports (L), over the cross area of the sample (thickness "*t*" and width "*w*"), as show in Eq. (2). Mechanical tests were performed using a universal testing machine (Instron 3366) under a crosshead speed of 0.2 mm/min at room temperature.

$$TRS = \frac{3 \cdot P \cdot L}{2 \cdot t2 \cdot w} \tag{2}$$

2.5. Microstructural evaluation

The microstructural characterization of consolidated Co-Cr-Mo and the fracture analysis were evaluated after tensile test. Metallography preparation consisted of mechanical grinding in SiC paper #1200 and final chemical polishing with OP-S 0.02 μm with addition of 10% HCl. The specimens were etching in solution: 100 ml HCl and 2 ml H_2O_2 (1–2 min at room temperature). The microstructural characterization was performed in both building directions using an optical microscope (OM) Olympus–BX51M and scanning electron microscope (SEM) with energy dispersive X-ray (EDS) Philips XL30 and JEOL–JSM6701F.

3. Results and discussion

3.1. Powder characterization

The confirmation of chemical composition was performed in Co-Cr-Mo powder alloy, as also in the samples manufactured (PC and SLM). The chemical composition is presented in **Table 2** comparing with the standard ASTM F75-12 [13].

Elements (%)	Powder	PC	SLM	ASTM F75
Co	63.93 ± 0.16	66.38 ± 0.15	65.38 ± 0.32	Balanço
Cr	28.83 ± 0.19	26.76 ± 0.21	27.68 ± 0.13	27.00 − 30.00 ± 0.30
Mo	7.07 ± 0.31	6.68 ± 0.03	6.61 ± 0.16	5.00 − 7.00 ± 0.15
Fe	0.17 ± 0.01	0.18 ± 0.08	0.33 ± 0.06	0.75 ± 0.03
C	0.03 ± 0.01	0.02 ± 0.01	0.03 ± 0.01	0.350 ± 0.020
S	0.01 ± 0.01	0.01 ± 0.01	0.01 ± 0.01	0.010 ± 0.003
N_2	0.0820 ± 0.0011	0.0416 ± 0.0015	0.1330 ± 0.0015	0.250 ± 0.020
O_2	0.0940 ± 0.0015	0.0187 ± 0.0016	0.0240 ± 0.0010	–

Table 2. Chemical composition (weight %) of Co-Cr-Mo samples (powder, PC and SLM) in accordance with standard ASTM F75.

The characteristic format of the powder process fabrication by gas atomization is observed in **Figure 7**. The analysis in SEM shows that the powders are spherical and presented satellites (appointed by arrows—**Figure 7a**,**b**). The satellites can be formed in the surface particles during the cooling process of the spherical powder particles during gas atomization. It is noteworthy that the shape of the particle influences on packing properties, flow hate, and compressibility, as well as reports on the powder metallurgy process [2, 57, 58]. The cross-sectioned powder (**Figure 7d**,**e**.) shows the dendritic morphology with the primarily arms and ramifications, characterizing the rapid solidification of gas atomization process.

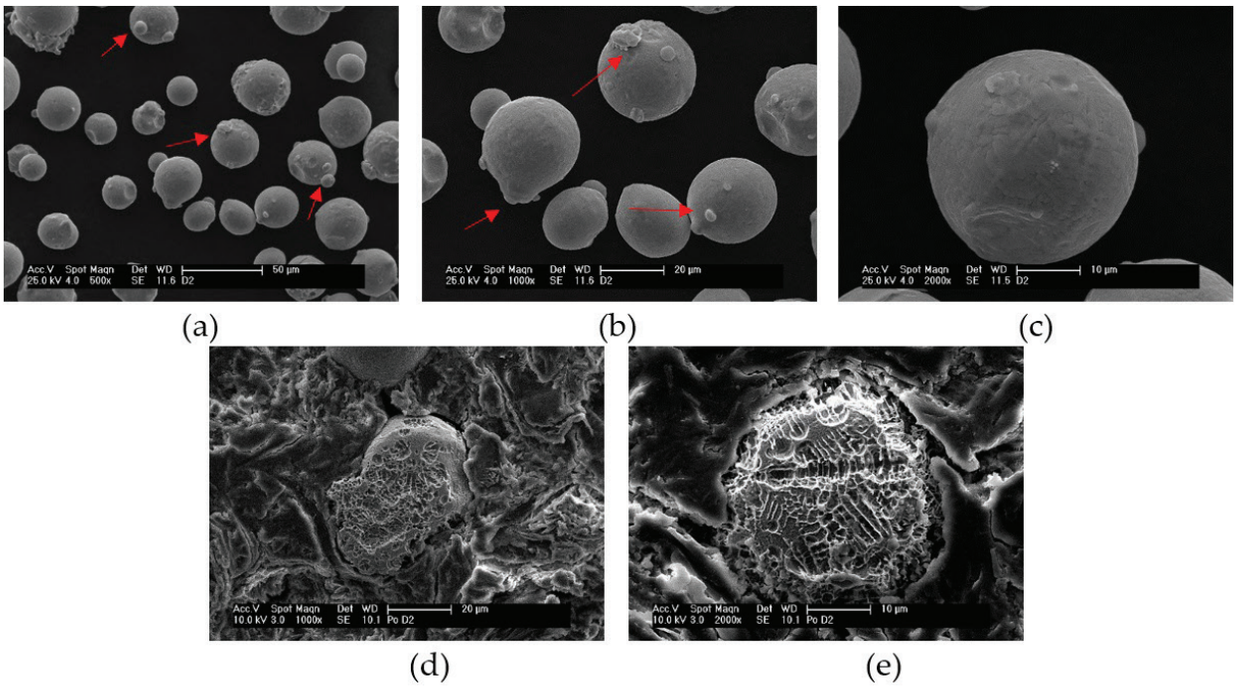

Figure 7. SEM images of Co-Cr-Mo powder: (a) magnitude ×500, (b) magnitude ×1000, (c) magnitude ×2000, (d) and (e) cross-section powder after chemical etch (etch solution: HCl, H_2SO_4, and HNO_3 for 60–240 s at 45°C, respectively, magnitude ×1000 and ×2000).

http://dx.doi.org/10.5772/intechopen.69720

Physical properties	Co-Cr-Mo powder			
Granulometric distribution (μm)	D10	D50	D90	D mean
	20.88	31.11	46.10	32.36
Flow rate (s/50g)	15.85 ± 0.11			
Apparent density (g/cm^3)	4.51 ± 0.01			
Tap density (g/cm^3)	5.26 ± 0.05			
Theoretical density (g/cm^3)	8.38			
Helium pycnometry (g/cm^3)	8.30 ± 0.001			

Table 3. Results of physical properties for Co-Cr-Mo powder in the SLM range.

The powders to manufacture samples via SLM technique have a mean diameter less than 50 μm to improve the physical properties such as flow time, apparent density, and tap density [33]. The results of physical powder properties are summarized in **Table 3**.

According to Haan et al. [59], Co-Cr-Mo powders with diameter D90 equals to 39 μm, the flowability was 18.60 s/50 g. The results were similar to those obtained for the present study, such as 15.86 s/50 g for D90 equals to 46.10 μm.

The result of tap density tends to be higher than the result of the apparent density, because of the particle's accommodation there is a decrease in the amount of voids between the particles [2]. Also, the smaller the apparent density, the greater the percentage of increase the tap density.

It is possible to verify the presence of closed porosity that is not considered as a measure of the volume of Helium and consequently reduces the value of pycnometry density (8.30 g/cm^3). The presence of internal porosity calculated in relation to theoretical density (8.38 g/cm^3) is approximately 1.3%.

To investigate and confirm the thermal events present in the Co-Cr-Mo alloy, the heating curves (different rates: 10, 20, and 30°C/min) of the DSC analysis obtained using the Co-Cr-Mo powder are shown in **Figure 8**. The presence of three events occurring in the heating curves of DSC is observed, being the first exothermic, the second endothermic, and the final event corresponding to the fusion of the Co-Cr-Mo alloy. It is possible to verify the temperature variation of the events between the different temperature rates.

In relation to the first event (exothermic), occurring around 582.81°C, it is related to the phase transformation of the alloy (precisely from Co), from the cubic face (αCo) phase to the compact hexagonal phase (εCo). In a similar analysis, Santos [16] obtained a slight peak at 600°C in the thermal analysis (DTA), however the author does not approach the occurrence. Facchini [60] describes this occurrence, the event occurs at approximately 650°C, but is described by an endothermic peak, diverging from the present analysis, in which the curve of 20°C/min occurs at approximately 600°C and which describes an exothermic peak.

The second event (endothermic) occurs around 944.52°C, may be related to allotropic transformation of element Co, by the transition of the phase of compact hexagonal structure (εCo) to the phase of cubic structure of face centered (αCo). This transformation can be confirmed

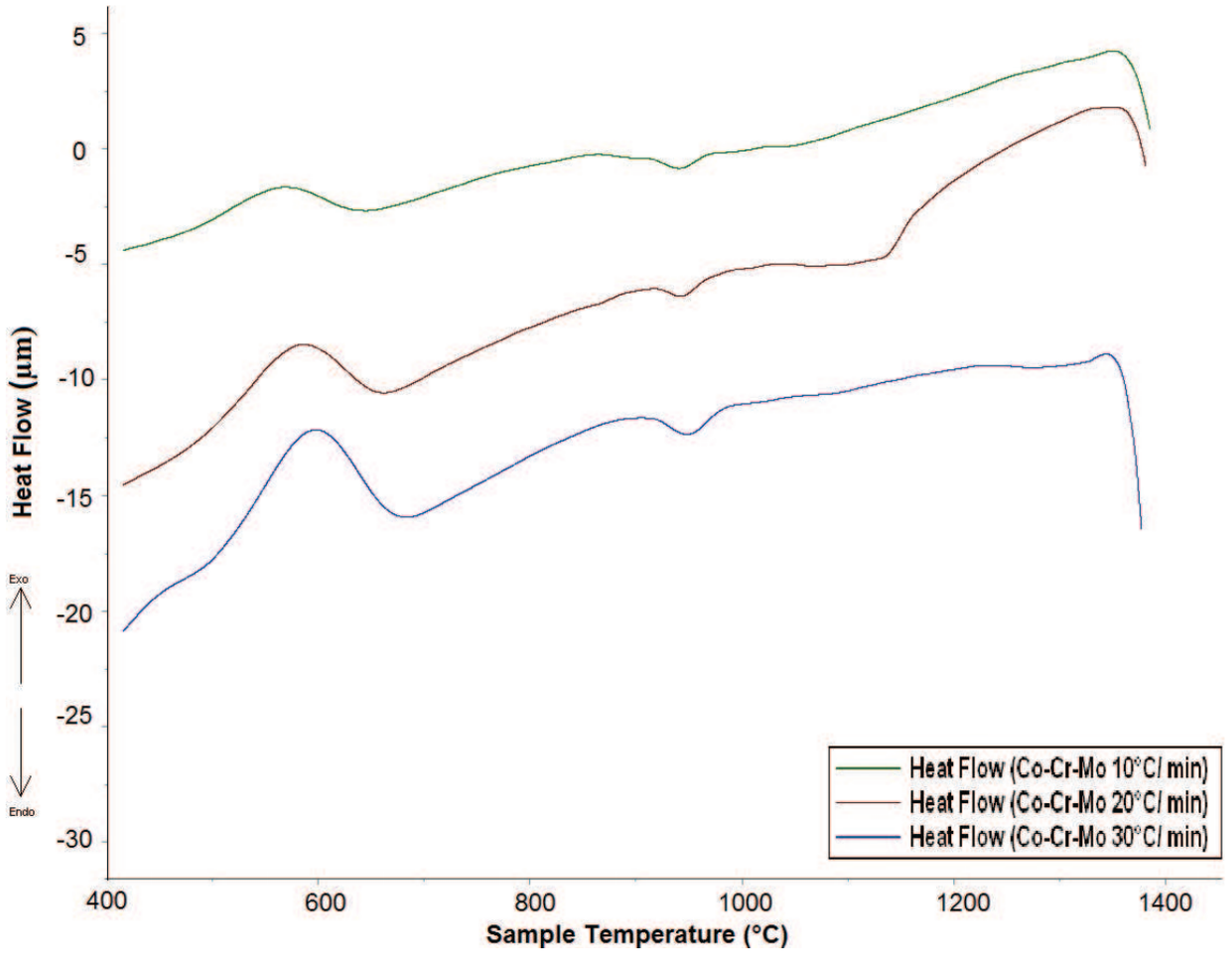

Figure 8. Heating curves of DSC analysis for Co-Cr-Mo powder in different rates (10, 20, and 30°C/min).

in the Co-Cr binary diagram occurring at about 950°C). This occurrence is similar to that described in Ref. [16, 60], which obtains endothermic peaks, respectively, at approximately 970 and 1000°C, relative to that obtained in the present study of 944.52°C. This temperature difference is associated with the chemical composition of the alloy (64Co-29Cr-7Mo of the present study), which represent alloys according to ASTM F75-12 (stoichiometry is 66Co-28Cr-6Mo) and therefore there are temperature difference of 26 and 56°C relative to the cited references. This difference can be associated to different calibrations, among the equipment used in the analysis.

In interpreting the DSC curves, it is possible to verify the melting temperature of the Co-Cr-Mo alloy. By means of the average value of the three heating rates, the melting temperature is approximately 1354.5°C, with a variation of 4°C between rates.

3.2. Evaluation of samples manufactured

The result of the cytotoxicity analysis for the processed samples is shown in **Figure 9**. According to the cytotoxicity assay with respect to the pure extract, without dilution, the samples processed by precision casting and selective laser melting showed no toxicity.

http://dx.doi.org/10.5772/intechopen.69720

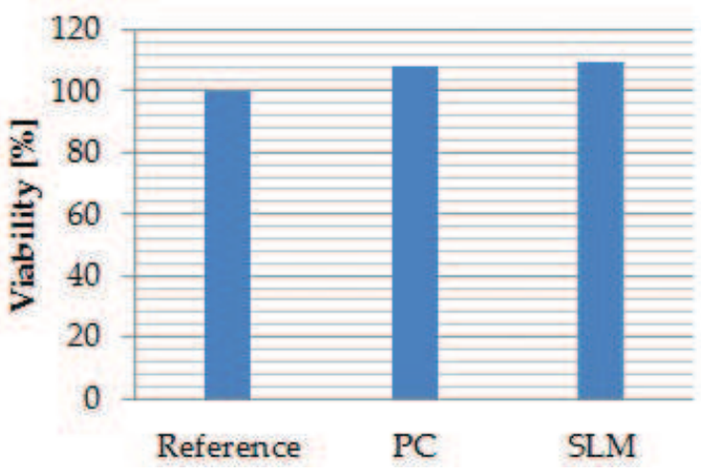

Figure 9. Result of viability of cell growth (cytotoxicity analysis) for Co-Cr-Mo specimens manufactured by PC and SLM techniques.

The results showed the expected results for the Co-Cr-Mo alloy, because as there is a need for specific mechanical properties to be reached, the use of Co-Cr alloys for the manufacture of medical and dental implants or prostheses did not show any toxicity with the medium biological [7, 8, 61].

The porosity of the samples was determined and a comparison was made with average densities: theoretical, volumetric, and by helium pycnometry. The results of the mean densities obtained for the samples consolidated by PC and SLM can be seen in **Table 4**.

Analyzing the results of volumetric density, it is possible to identify that PC samples present a lower result than the one obtained in the SLM samples. This premise is confirmed by the result obtained, evidencing that the PC process presents superior open porosity than SLM technology. When correlating with the density by Helium pycnometry, it can be verified that the open porosity results in 0.24% for PC sample and 0.12% for SLM sample.

Analyzing the Helium pycnometry, it is possible to verify that both consolidation processes have the same theoretical density (8.24 g/cm^3). Relating the Helium pycnometry density to the theoretical density is possible to check the internal porosity, that results, respectively, for the PC and SLM process of 2.14 and 1.80%. It can be concluded that the SLM consolidation process produces samples with lower internal porosity, and can obtain components with densities around 98.20% of theoretical, in contrast to the PC process that obtains components with density of 97.86% of theoretical.

The heating curves obtained from TMA in the form of PC and SLM sample are presented in **Figure 10**. To understand the events occurred at TMA, the heating curves of DSC analysis were juxtaposed. The CTE for the consolidated samples has a different behavior between the processes of the Co-Cr-Mo alloy in a similar analysis to the present study. The CTE for the consolidated samples has a distinct behavior between the processes of the Co-Cr-Mo alloy. As it is possible to verify the CTE at temperature of 500°C of samples (SLM 1, SLM 2, and PC) is, respectively, 15.0/19.5/22.0 × 10^{-6} °C^{-1}. At the temperature of 600°C, the coefficient value decreases to the values of 12.5/14.5/18.5 × 10^{-6} °C^{-1}. This difference is greater for the

Sample	Densities (g/cm³)		
	Theoretical	Helium pycnometry	Volumetric
PC	8.42	8.24 ± 0.01	8.22 ± 0.10
SLM	8.39	8.24 ± 0.01	8.23 < 0.01

Table 4. Results of densities (medium values): theoretical, Helium pycnometry and volumetric for samples PC and SLM.

alloy processed by PC, which is associated to the dendritic microstructure formed and in relation to the casting process because it characterizes a fine grain microstructure and more packaging.

As can be seen in the TMA and DSC curves are similar in the temperature ranges of events. Facchini [60] shows the DSC and TMA curves (heating rate of 20°C/min) performed in an ASTM F75-12 composition alloy and processed by electron beam fusion (EBM). EBM has an effect similar to the SLM because both processes have a concentrated heat source and is possible to relate the DSC analysis, in which, the first peak (565–900°C) is associated with the transition from the FCC (αCo) phase to the HCP (εCo) phase, and the second peak (900–1000°C) reduces the HCP phase (εCo) and reappearance of the FCC phase (αCo).

Is possible observed two events, the first event occurs in the range of 514–614°C and the second event at 923–961°C. In the case of the PC sample (TMA curve), it is possible to verify that the events occur in a higher temperature in relation to the samples processed by SLM. This occurrence is associated to the microstructure samples of analysis performed. The powder

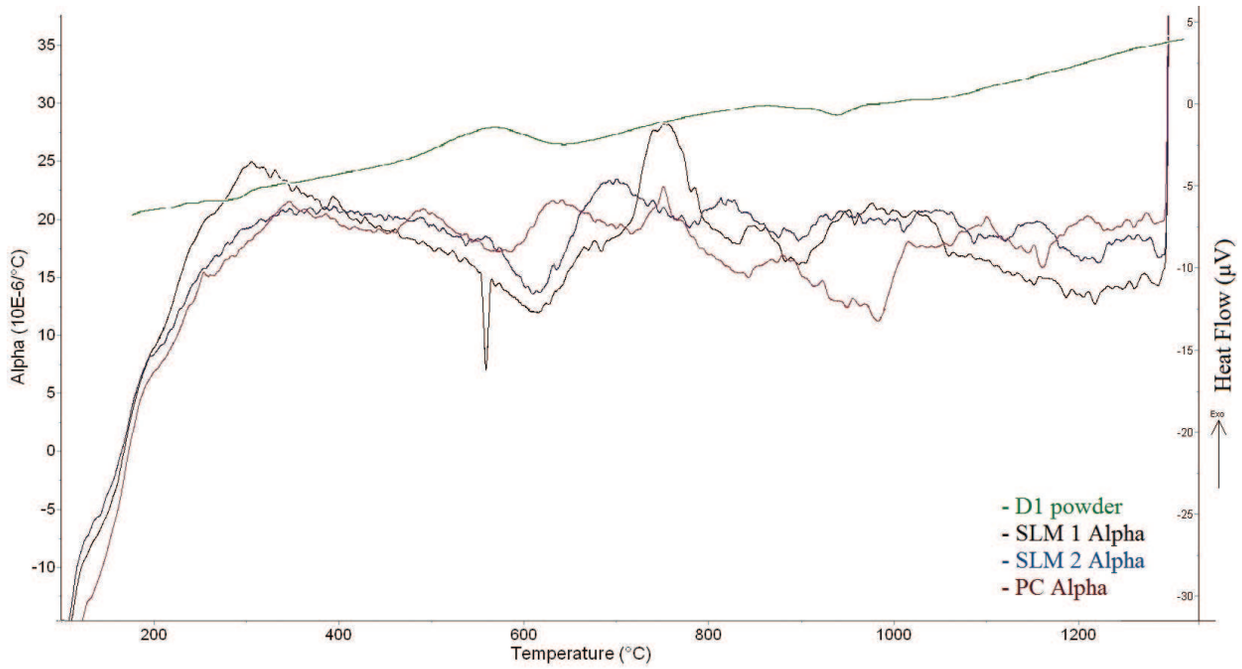

Figure 10. Heat curve of thermal analysis for Co-Cr-Mo samples: DSC curve of Co-Cr-Mo powder sample and TMA curves of consolidated samples PC and SLM (SLM 1 and SLM 2).

sample (at DSC analysis) has a dendritic microstructure, as the same of the PC sample (at TMA). TMA curves of SLM samples (SLM 1 and SLM 2) show more evident peaks, but the transition of these events set at increased temperatures. Thus, the laser fusion process has a refined and more homogeneous microstructure what hinders phase transitions and requires higher temperatures.

3.3. Mechanical behavior

The mechanical results of the tests for the PC and SLM specimens are present in **Table 5**. Analyzing the values is possible to verify that in all properties the SLM technique results in higher properties than PC technique. According to standard ISO22674:06 [54], the SLM and PC specimens satisfied the type 5 criteria in all mechanical properties.

The result of TRS samples (SLM = 2501.2 ± 9.7 MPa and PC = 1072.3 ± 4.6 MPa) was satisfactory. However, there was no rupture of PC sample (test interrupted) evidenced the ductility of the precision casting process, that was confirmed by the value of higher elongation. According to Mengucci et al. [62], the TRS result for a similar composition of Co-Cr-Mo alloy, after the shoot-peened treatment followed by heat treatment for strain relief, resulted a TRS equal to 2700 ± 25 MPa. Therefore, the present results are acceptable comparing the data obtained with the study by Mengucci et al. [62].

The heat treatment, as hot isostatic pressing (HIP), after the additive manufacturing process (by laser melting process–SLM and EBM) of parts has been used successfully by medical and aeronautic manufactures. The HIP process is effective to obtain better results of mechanical properties (ductility and fatigue resistance) and decrease the porosity [60, 63]. Although this present study evaluated the mechanical properties of SLM and PC samples without any post-process of heat treatment is possible, check the relevant mechanical properties obtained by manufacture process. According to the results present evaluation is presented in **Table 6** to compare the mechanical properties to those presented in the literature [14, 41, 44, 62, 64].

Mechanical properties	Consolidation technique		Standards	
	PC	SLM	ISO 22674 "type 5"	ASTM F75 "casting"
Yield strength (MPa)	646.7 ± 44.4	731.5 ± 40.3	500	450
Rupture strength (MPa)	742.2 ± 106.8	1127.9 ± 0.1	–	–
Ultimate tensile strength (MPa)	771.7 ± 103.3	1136.9 ± 1.0	–	655
Elongation (%)	14.20 ± 2.8	13.7 ± 5.3	2	8
Elastic modulus "E" (GPa)	223.42 ± 15.7	225.2 ± 14.4	150	–
Hardness Vickers (HV)	272.2 ± 20.5	334.8 ± 16.0	–	266–345
TRS (MPa)	1072.3 ± 4.6	2501.2 ± 9.7	–	–

Table 5. Mechanical properties of Co-Cr-Mo alloy manufactured by PC and SLM compared to the minimum properties required by standards.

References		Alloy (wt%)	σ_{YS} (MPa)	El (%)	σ_{UTS} (MPa)	TRS (MPa)	Hardness (HV)
Present work Co-Cr-Mo	PC	64Co-29Cr-7Mo	646.76 ± 44.36	14.20 ± 2.76	771.70 ± 103.32	1072.3 ± 4.6	256.7 ± 12.9
	SLM		731.50 ± 40.31	13.73 ± 5.32	1136.95 ± 0.92	2501.2 ± 9.7	358.1 ± 9.8
Takaichi et al. [64]	C	Co-28Cr-6Mo	296 ± 25	9.6 ± 2.5	912 ± 39	–	–
	SLM		516 ± 28	10.7 ± 2.9	591 ± 37	–	–
Qian et al. [41]	C	60-65Co 26-30Cr 5-7Mo	610	–	741	–	–
	SLM		873 ± 76	–	1303 ± 73	–	–
Kajima et al. [44]	C	63Co-29Cr-6Mo	571 ± 23	11.2 ± 2	775 ± 67	–	–
	SLM	60-65Co 26-30Cr 5-7Mo	877 ± 37	12.3 ± 3	1170 ± 29	–	–
Mengucci et al. [62]	SLM	63.8Co-24.7Cr-5.1Mo-5.4W	–	–	1340 ± 20	2700 ± 25	434 ± 22
Jabbari et al. [14]	C	61.6Co-30Cr-6.5Mo	–	–	–	–	320 ± 12
	SLM	Co-29Cr-5.5Mo	–	–	–	–	371 ± 10
Liverani et al. [40]	SLM	Co 27-30Cr 5-7Mo	677	–	–	–	361 ± 31

Table 6. Comparative results for mechanical properties obtained in the present study with Co-Cr alloys manufactured by selective laser melting (SLM) and casting (C) process presented in the literature.

3.4. Microstructural analysis

To understand the mechanical properties improved in the SLM specimens in relation to the casting process technique carried out the microstructural analysis by OM and SEM-EDS.

The microstructural analysis by OM of PC samples (**Figure 11a,b**) describe dendritic arms and ramifications with different solidification orientations [14]. In addition, PC sample present porous (microporous) as the SLM samples, but are uneven (a little larger but in small quantity). This occurrence is possible to form by problems of dispersing the powder in the bed layer and the presence of satellites/porous in the powder particles. SLM specimens show a characteristic morphology (weld-like structure) of laser beam melting. Is possible to check the layers formed during the manufacture process (**Figure 11c,d**)? The vertical section of SLM sample is to observe the building direction of specimen (indicated by arrow—**Figure 11d**) characterized by the overlapping of each layer and the morphology formation by the action of the laser beam such as the weld pool.

Figure 12 represents the SEM images of PC samples and the semi-quantitative analysis of interesting points by EDS. It is possible to identify the cast specimen with a second phase (white area) in the matrix. The semi-quantitative analysis with the EDS and the respective spectrums (**Figure 12c,d**) show that the composition of white area (point 1) is rich in Mo element, and the matrix (point 2) is composed by Co-Cr elements, with a small percentage of Mo. The phase (point 1) shows the confirmation of carbide ($M_{23}C_6$) presence, rich in chromium and

http://dx.doi.org/10.5772/intechopen.69720

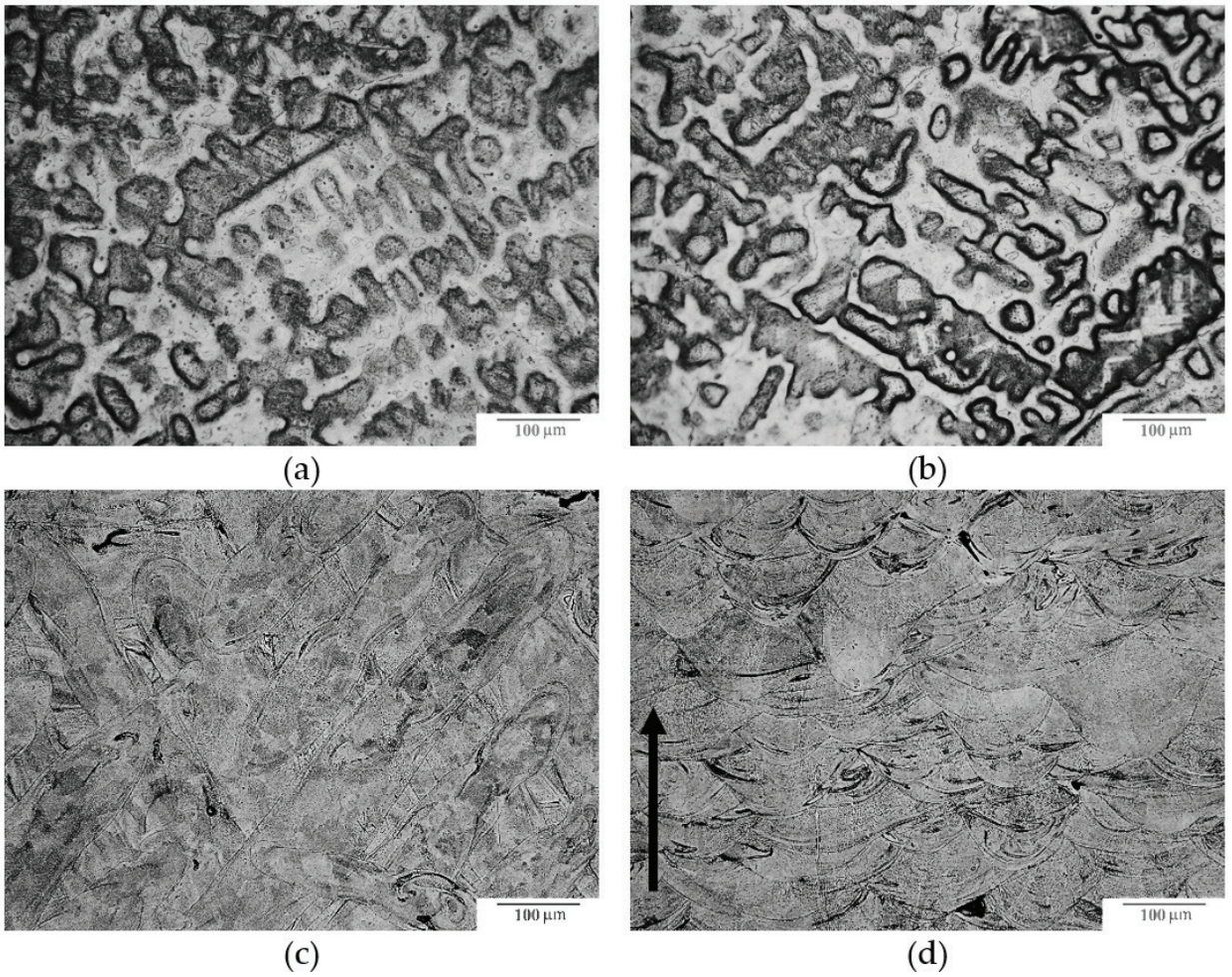

Figure 11. MO images of Co-Cr-Mo alloy consolidated: (a–b) transversal and longitudinal view of precision casting sample and (c–d) transversal and longitudinal (arrow indicates building consolidation) view of selective laser melting (Etch: 100 ml HCl and 2 ml H_2O_2. Magnitude: ×200).

molybdenum [14]. The $M_{23}C_6$ carbide results in a micro hardness of 699 ± 131 HV (1 mN/15 s) in opposition of 338 ± 14 HV (1 mN/15 s) to the micro hardness of matrix.

Figure 13 shows the microstructure of SLM specimen. It is observed that a microstructure is formed with small grains characterizing the rapid solidification during the SLM manufacturing process. The semi-quantitative analysis in the fine grains shows that it does not have different elements compositions. SLM specimen presents a homogeneous matrix with Co-Cr-Mo elements. The morphology formation of the laser melting sample was also observed after electrolytic attack [59, 61]. Also confirms that the fine grains are oriented in direction of the laser scanning. This characteristic microstructure of laser melting technique allows to achieve better mechanical properties than the cast technique.

The fractures of the tensile samples were SEM analyzed (**Figure 14**) observed the formation of dimples homogeneously distributed in the microfracture of both samples. Regions with the presence of dimples are ductless and with higher toughness. However, it is apparent that the dimple formations on the SLM sample extends completely by the fracture planes and are of

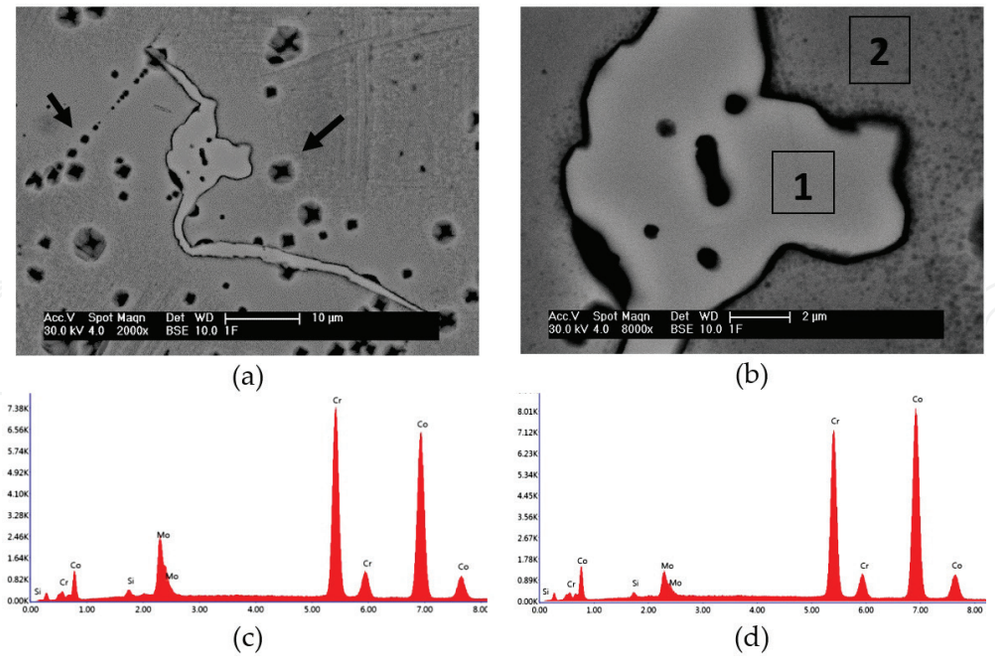

Figure 12. SEM images of PC sample: (a) magnitude ×2000, (b) magnitude ×8000, and (c–d) EDS spectrograms of analysis at point 1 and point 2.

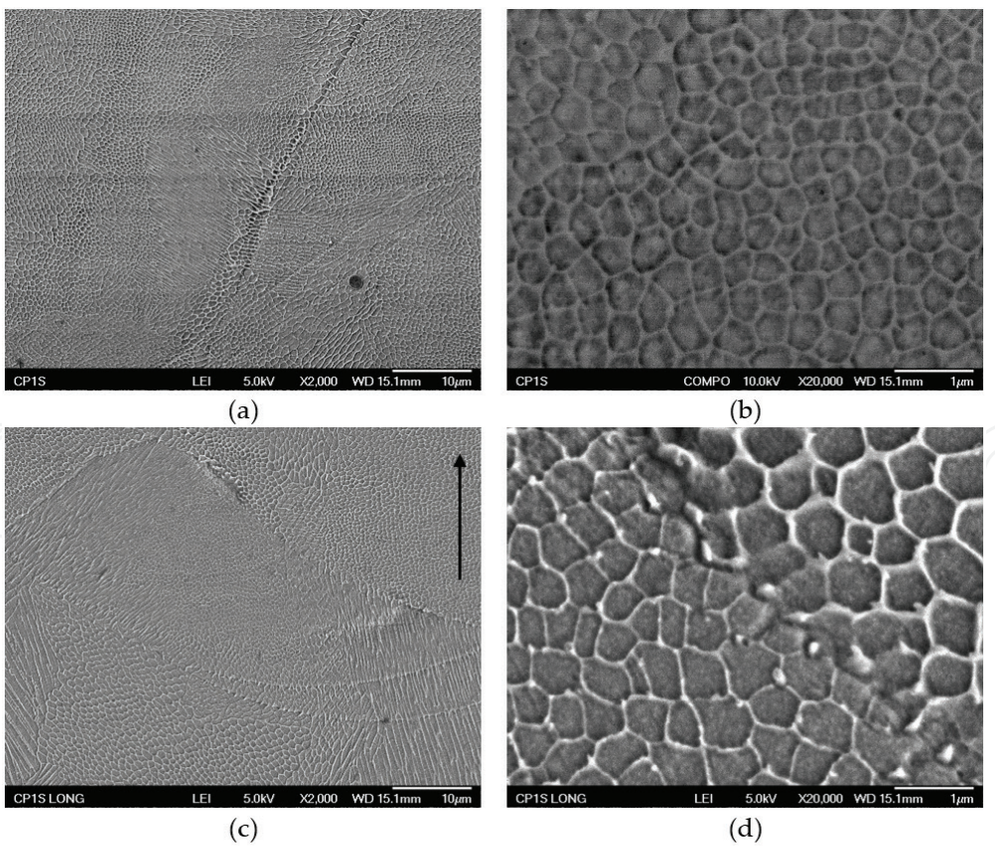

Figure 13. SEM images of SLM specimens: (a) horizontal section from backscattered electrons, and (b) from secondary electrons, (c–d) vertical section from backscattered electrons (black arrow indicates the building consolidation).

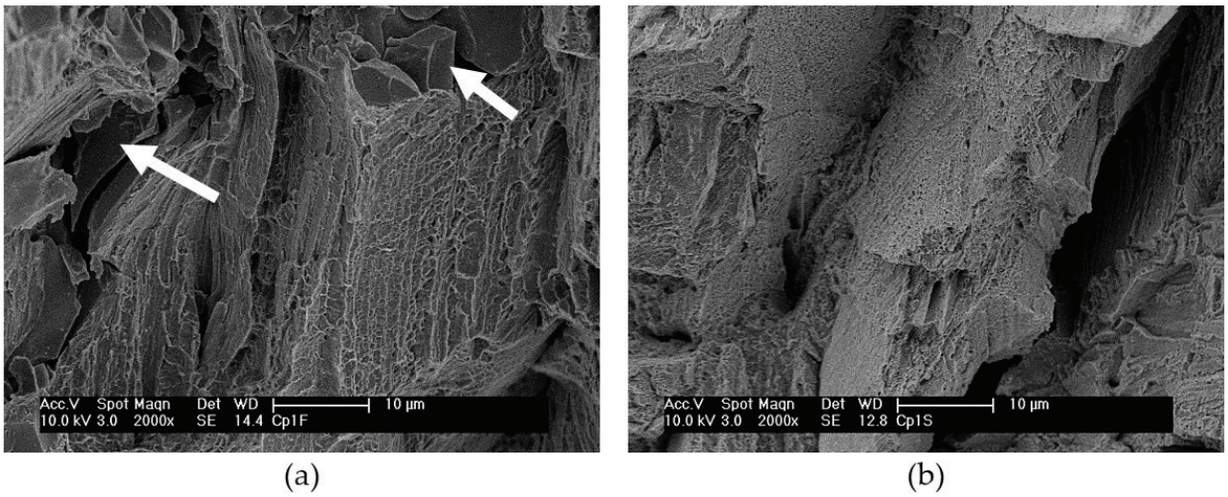

Figure 14. SEM images of tensile fracture: (a) PC sample and (b) SLM sample (magnitude: ×2000).

finer size, compared to the fracture with dimples geometrically larger of PC sample. It can be verified with SLM samples and confirmed with the mechanical results in relation to PC samples. In addition, some planar regions (indicated by arrows) show a semi-cleavage morphology. The type of fracture observed in the samples, according to Takaichi et al. [64], describes the formation of dimples along the fracture surface, as well as cracking of the wedge is appointed as a possible formation of cleavage fracture over favorable crystallographic planes.

4. Conclusions

In general, the results of powders characterization showed that the granulometric range of 20–50 μm is the one that best fits in the properties of packaging, for the consolidation by SLM.

The biocompatibility of the samples obtained a positive result for both processing techniques. In this way, the development of the present study evidenced to improve the manufacture of customized dental components (copings) using the SLM technique.

Microstructural analysis obtained for SLM samples results in a characteristic morphology of layer manufacturing with ultrafine grains and a high chemical homogeneity. The conventional technique presented a differentiated microstructure by the gross dendritic microstructure of casting process.

The mechanical evaluation showed that the SLM technique provides superior mechanical properties (as yield strength, rupture strength, ultimate tensile strength, TRS, and hardness) compared to those obtained by the precision casting technique.

The thermal analyses showed the present phase transitions of Co-Cr-Mo alloy, as well as being possible to correlate them (TMA to DSC curves). The coefficient of thermal expansion (CTE) resulted for both processes a similar value to alloys used in dental materials.

The processing using laser melting proved better mechanical and thermal properties to precision casting processing technique without post-processing (thermal treatment). SLM technique evidenced a promising use to manufacture prosthetics and dental implants. Nevertheless, it is still of great concern and promising further development of laser melting process (SLM and EBM) in relation to the parameters and variables of process, as also to the post-processing method apply to AM parts. Such characteristics should be addressed to new materials and investigate in relation to the performance and bio-functionality of specific application part.

Acknowledgements

This study was financially support by CNPq and FAPESP. The authors also thank to Ms. Amed Belaid and SLM® Solution for SLM specimens and collaboration.

Author details

Marcello Vertamatti Mergulhão*, Carlos Eduardo Podestá and
Maurício David Martins das Neves

*Address all correspondence to: marcellovertamatti@gmail.com

Nuclear and Energy Research Institute (IPEN/CNEN-SP), CCTM, São Paulo, Brazil

References

[1] Davis JR, editor. ASM Specialty Handbook: Nickel, Cobalt, and Their Alloys. 1st ed. ASM International; Materials Park, OH, 2000. p. 442

[2] Lee PW, editor. Powder Metal Technologies and Applications. Vol. 7. 9th ed. ASM International; Materials Park, OH, 1998. p. 1147

[3] Misch CE. Dental Implant Prosthetics. 2nd ed. Elsevier; Missouri, 2015. p. 1008

[4] Ivanova EP, Bazaka K, Crawford RJ. Cytotoxicity and biocompatibility of metallic biomaterials. In: New Funct. Biomater. Med. Healthc. Elsevier; Cambridge, 2014. pp. 148-172. DOI: 10.1533/9781782422662.148

[5] Ratner BD, Hoffman AS, Schoen FJ, Lemons JE. Biomaterials Science: An Introduction to Materials in Medicine. 2nd ed. Academic Press; San Diego, California, 2004. p. 864. ISBN: 9780080470368

[6] McCabe JF, Walls AWG, editors. Applied Dental Materials. 9th ed. Blackwell Publishing Ltd.; Oxford, 2008. p. 312. ISBN: 978-1-118-69712-2

[7] Wataha JC. Biocompatibility of dental casting alloys: A review. The Journal of Prosthetic Dentistry. 2000;**83**:223-234. DOI: 10.1016/S0022-3913(00)80016-5

[8] Kim HR, Kim YK, Son JS, Min BK, Kim KH, Kwon T-Y. Comparison of in vitro biocompatibility of a Co-Cr dental alloy produced by new milling/post-sintering or traditional casting technique. Materials Letters. 2016;**178**:300-303. DOI: 10.1016/j.matlet.2016.05.053

[9] Hedberg YS, Qian B, Shen Z, Virtanen S, Wallinder IO. In vitro biocompatibility of CoCrMo dental alloys fabricated by selective laser melting. Dental Materials. 2014;**30**:525-534. DOI: 10.1016/j.dental.2014.02.008

[10] Borelli V. Pesquisa e desenvolvimento de biomateriais: estudo das inter-relações científicas, tecnológicas e normativas. [Master]. São Paulo: Instituto de Pesquisas Energéticas e Nucleares (IPEN/USP); 2011

[11] Williams DF. On the mechanisms of biocompatibility. Biomaterials. 2008;**29**:2941-2953. DOI: 10.1016/j.biomaterials.2008.04.023

[12] Niinomi M, Narushima T, Nakai M, editors. Advances in Metallic Biomaterials. Vol. 3. Berlin, Heidelberg: Springer Berlin Heidelberg; 2015. p. 348. DOI: 10.1007/978-3-662-46836-4

[13] ASTM F75-12. Standard Specification for Cobalt-28 Chromium-6 Molybdenum Alloy Castings and Casting Alloy for Surgical Implants (UNS R30075). West Conshohocken, PA: ASTM International; 2012

[14] Jabbari YSA, Koutsoukis T, Barmpagadaki X, Zinelis S. Metallurgical and interfacial characterization of PFM Co-Cr dental alloys fabricated via casting, milling or selective laser melting. Dental Materials. 2014;**30**:e79-e88. DOI: 10.1016/j.dental.2014.01.008

[15] Oyagüe RC, Sánchez-Turrión A, López-Lozano JF, Montero J, Albaladejo A, Suárez-García MJ. Evaluation of fit of cement-retained implant-supported 3-unit structures fabricated with direct metal laser sintering and vacuum casting techniques. Odontology. 2012;**100**:249-253. DOI: 10.1007/s10266-011-0050-1

[16] Santos LA. Processamento e caracterização da liga 66Co-28Cr-6Mo (% peso) para implantes. [Master]. São Paulo: Universidade de São Paulo; 2012

[17] Craig RG. Craig's Restorative Dental Materials. 13th ed. Elsevier/Mosby; Philadelphia, 2012. p. 416

[18] Ren L, Memarzadeh K, Zhang S, Sun Z, Yang C, Ren G, et al. A novel coping metal material CoCrCu alloy fabricated by selective laser melting with antimicrobial and antibiofilm properties. Materials Science and Engineering C. 2016;**67**:461-467. DOI: 10.1016/j.msec.2016.05.069

[19] van Noort R. The future of dental devices is digital. Dental Materials. 2012;**28**:3-12. DOI: 10.1016/j.dental.2011.10.014

[20] Utela B, Storti D, Anderson R, Ganter M. A review of process development steps for new material systems in three dimensional printing (3DP). Journal of Manufacturing Processes. 2008;**10**:96-104. DOI: 10.1016/j.jmapro.2009.03.002

[21] Örtorp A, Jönsson D, Mouhsen A, von Steyern PV. The fit of cobalt-chromium three-unit fixed dental prostheses fabricated with four different techniques: A comparative in vitro study. Dental Materials. 2011;**27**:356-363. DOI: 10.1016/j.dental.2010.11.015

[22] Li KC, Prior DJ, Waddell JN, Swain MV. Comparison of the microstructure and phase stability of as-cast, CAD/CAM and powder metallurgy manufactured Co-Cr dental alloys. Dental Materials. 2015;**31**:e306-e315. DOI: 10.1016/j.dental.2015.10.010

[23] Bilgin MS, Erdem A, Dilber E, Ersoy İ. Comparison of fracture resistance between cast, CAD/CAM milling, and direct metal laser sintering metal post systems. Journal of Prosthodontic Research. 2016;**60**:23-28. DOI: 10.1016/j.jpor.2015.08.001

[24] Kale PJ, Metkar RM, Hiwase SD. Development and optimization of dental crown using rapid prototyping integrated with CAD. In: Wimpenny DI, Pandey PM, Kumar LJ, editors. In: Advanced 3D Printing and Additive Manufacturing Technology. Singapore: Springer Singapore; 2017. pp. 169-182. DOI: 10.1007/978-981-10-0812-2_15

[25] Shah P, Racasan R, Bills P. Comparison of different additive manufacturing methods using computed tomography. Case Studies in Nondestructive Testing and Evaluation. 2016;**6**:69-78. DOI: 10.1016/j.csndt.2016.05.008

[26] Gibson I. Advanced Manufacturing Technology for Medical Applications: Reverse Engineering, Software Conversion and Rapid Prototyping. John Wiley & Sons Ltd, Chichester, UK, 2005

[27] Grzesiak D, Krawczyk M. Effects of the selective laser melting process parameters on the functional properties of the Co-Cr alloy. International Journal of Recent Contributions from Engineering, Science & IT (iJES). 2015;**3**:39-42. DOI: 10.3991/ijes.v3i1.4291

[28] Germanovix AA. Establishing a benchmark part to analyze the capabilities of selective laser melting systems. [Bacharel]. Universidade Federal de Santa Catarina: Santa Catarina, Brasil, 2011

[29] Bremen S, Meiners W, Diatlov A. Selective laser melting: A manufacturing technology for the future? Laser Technik Journal. 2012;**9**:33-38. DOI: 10.1002/latj.201290018

[30] Yap CY, Chua CK, Dong ZL, Liu ZH, Zhang DQ, Loh LE, et al. Review of selective laser melting: Materials and applications. Applied Physics Reviews. 2015;**2**:041101. DOI: 10.1063/1.4935926

[31] Meiners W. Selective Laser Melting: Generative Fertigung fur die Produktion der Zukunft Optische Technologien in der Produktionstechnik. Aachen: Fraunhofer Institut fur Lasertechnik: 2012

[32] Gu DD, Meiners W, Wissenbach K, Poprawe R. Laser additive manufacturing of metallic components: Materials, processes and mechanisms. International Materials Reviews. 2012;**57**:133-164. DOI: 10.1179/1743280411Y.0000000014

[33] Kurzynowski T, Chlebus E, Kuźnicka B, Reiner J. Parameters in selective laser melting for processing metallic powders. In: Beyer E, Morris T, editors; 2012. pp. 823-914. DOI: 10.1117/12.907292

[34] Sallica-Leva E, Jardini AL, Fogagnolo JB. Microstructure and mechanical behavior of porous Ti-6Al-4V parts obtained by selective laser melting. Journal of the Mechanical Behavior of Biomedical Materials. 2013;**26**:98-108. DOI: 10.1016/j.jmbbm.2013.05.011

[35] Simchi A, Pohl H. Effects of laser sintering processing parameters on the microstructure and densification of iron powder. Materials Science and Engineering A. 2003;**359**:119-128. DOI: 10.1016/S0921-5093(03)00341-1

[36] Calignano F, Manfredi D, Ambrosio EP, Biamino S, Lombardi M, Atzeni E, et al. Overview on additive manufacturing technologies. Proceedings of IEEE. 2017:1-20. DOI: 10.1109/JPROC.2016.2625098

[37] Zhou X, Liu X, Zhang D, Shen Z, Liu W. Balling phenomena in selective laser melted tungsten. Journal of Material Processing Technology. 2015;**222**:33-42. DOI: 10.1016/j.jmatprotec.2015.02.032

[38] Gu D, Shen Y. Balling phenomena in direct laser sintering of stainless steel powder: Metallurgical mechanisms and control methods. Materials & Design. 2009;**30**:2903-2910. DOI: 10.1016/j.matdes.2009.01.013

[39] Senthilkumaran K, Pandey PM, Rao PVM. Influence of building strategies on the accuracy of parts in selective laser sintering. Materials & Design. 2009;**30**:2946-2954. DOI: 10.1016/j.matdes.2009.01.009

[40] Liverani E, Fortunato A, Leardini A, Belvedere C, Siegler S, Ceschini L, et al. Fabrication of Co-Cr-Mo endoprosthetic ankle devices by means of Selective Laser Melting (SLM). Materials & Design. 2016;**106**:60-68. DOI: 10.1016/j.matdes.2016.05.083

[41] Qian B, Saeidi K, Kvetková L, Lofaj F, Xiao C, Shen Z. Defects-tolerant Co-Cr-Mo dental alloys prepared by selective laser melting. Dental Materials. 2015;**31**:1435-1444. DOI: 10.1016/j.dental.2015.09.003

[42] Cheng B, Shrestha S, Chou K. Stress and deformation evaluations of scanning strategy effect in selective laser melting. Additive Manufacturing. 2016;**12**:240-251. DOI: 10.1016/j.addma.2016.05.007

[43] Alsalla H, Hao L, Smith C. Fracture toughness and tensile strength of 316L stainless steel cellular lattice structures manufactured using the selective laser melting technique. Materials Science and Engineering A. 2016;**669**:1-6. DOI: 10.1016/j.msea.2016.05.075

[44] Kajima Y, Takaichi A, Nakamoto T, Kimura T, Yogo Y, Ashida M, et al. Fatigue strength of Co-Cr-Mo alloy clasps prepared by selective laser melting. Journal of the Mechanical Behavior of Biomedical Materials. 2016;**59**:446-458. DOI: 10.1016/j.jmbbm.2016.02.032

[45] Simonelli M, Tse YY, Tuck C. Effect of the build orientation on the mechanical properties and fracture modes of SLM Ti-6Al-4V. Materials Science and Engineering A. 2014;**616**:1-11. DOI: 10.1016/j.msea.2014.07.086

[46] Džugan J, Nový Z. Powder Application in Additive Manufacturing of Metallic Parts. In: Dobrzanski LA, editor. Powder Metallurgy - Fundamentals and Case Studies [Internet]. InTech; Rijeka, Croatia, 2017

[47] Sun YY, Gulizia S, Oh CH, Doblin C, Yang YF, Qian M. Manipulation and characterization of a novel titanium powder precursor for additive manufacturing applications. JOM. 2015;**67**:564-572. DOI: 10.1007/s11837-015-1301-3

[48] Tang HP, Qian M, Liu N, Zhang XZ, Yang GY, Wang J. Effect of powder reuse times on additive manufacturing of Ti-6Al-4V by selective electron beam melting. JOM. 2015;**67**:555-563. DOI: 10.1007/s11837-015-1300-4

[49] Slotwinski JA, Garboczi EJ, Stutzman PE, Ferraris CF, Watson SS, Peltz MA. Characterization of metal powders used for additive manufacturing. Journal of Research of the National Institute of Standards and Technology. 2014;**119**:460. DOI: 10.6028/jres.119.018

[50] Gaytan SM, Murr LE, Medina F, Martinez E, Lopez MI, Wicker RB. Advanced metal powder based manufacturing of complex components by electron beam melting. Materials Technology. 2009;**24**:180-190. DOI: 10.1179/106678509X12475882446133

[51] ASTM International. B212-13—Standard Test Method for Apparent Density of Free-Flowing Metal Powders Using the Hall Flowmeter Funnel. Pensilvânia: ASTM; 2013

[52] ASTM International. B213-13—Standard Test Methods for Flow Rate of Metal Powders Using the Hall Flowmeter Funnel. Pensilvânia: ASTM; 2013

[53] ASTM International. B527-14—Standard Test Method for Determination of Tap Density of Metal Powders and Compounds. Pensilvânia: ASTM; 2014

[54] ISO. 22674-06—Dentistry—Metallic Materials for Fixed and Removable Restorations and Appliances. Geneva: ISO, 2006

[55] ASTM International. B528-12—Standard Test Method for Transverse Rupture Strength of Powder Metallurgy (PM) Specimens. Pensilvânia: ASTM; 2012

[56] ISO. 10933-5—Biological Evaluation of Medical Devices—Part 5: Tests for Cytotoxicity: In Vitro Methods; 1995

[57] German RM. Powder Metallurgy Science. 2nd ed. Princeton: Metal Powder Industry Federation; 1994

[58] Gessinger GH. Powder Metallurgy of Superalloys. Baden, Switzerland: Butterworth & Co.; 1984

[59] Haan J, Asseln M, Zivcec M, Eschweiler J, Radermacher R, Broeckmann C. Effect of subsequent hot isostatic pressing on mechanical properties of ASTM F75 alloy produced by Selective Laser Melting. Powder Metallurgy. 2015;**58**:161-165. DOI: 10.1179/0032589915Z.000000000236

[60] Facchini L. Microstructure and Mechanical Properties of Biomedical Alloys produced by Rapid Manufacturing Techniques. Doutorado: University of Trento; 2010

[61] Xin XZ, Xiang N, Chen J, Wei B. In vitro biocompatibility of Co-Cr alloy fabricated by selective laser melting or traditional casting techniques. Materials Letters. 2012;**88**:101-103. DOI: 10.1016/j.matlet.2012.08.032

[62] Mengucci P, Barucca G, Gatto A, Bassoli E, Denti L, Fiori F, et al. Effects of thermal treatments on microstructure and mechanical properties of a Co-Cr-Mo-W biomedical alloy produced by laser sintering. Journal of the Mechanical Behavior of Biomedical Materials. 2016;**60**:106-117. DOI: 10.1016/j.jmbbm.2015.12.045

[63] Benedetti M, Torresani E, Leoni M, Fontanari V, Bandini M, Pederzolli C, et al. The effect of post-sintering treatments on the fatigue and biological behavior of Ti-6Al-4V ELI parts made by selective laser melting. Journal of the Mechanical Behavior of Biomedical Materials. 2017;**71**:295-306. DOI: 10.1016/j.jmbbm.2017.03.024

[64] Takaichi A, Suyalatu, Nakamoto T, Joko N, Nomura N, Tsutsumi Y, et al. Microstructures and mechanical properties of Co-29Cr-6Mo alloy fabricated by selective laser melting process for dental applications. Journal of the Mechanical Behavior of Biomedical Materials. 2013;**21**:67-76. DOI: 10.1016/j.jmbbm.2013.01.021

IntechOpen

IntechOpen

IntechOpen